

## Core chemotype diversification in the HIV-1 entry inhibitor class using field-based bioisosteric replacement



Marina Tuyishime<sup>a</sup>, Rae Lawrence<sup>b</sup>, Simon Cocklin<sup>a,\*</sup>

<sup>a</sup> Department of Biochemistry & Molecular Biology, Drexel University College of Medicine, Rooms 10302–10306, 245 N. 15th Street, Philadelphia, PA 19102, USA

<sup>b</sup> Cresset, New Cambridge House, Bassingbourn Road, Litlington, Cambridgeshire, UK

### ARTICLE INFO

#### Article history:

Received 11 September 2015

Revised 23 October 2015

Accepted 26 October 2015

Available online 27 October 2015

#### Keywords:

Computer-aided drug design

HIV-1 envelope protein

Field-based

Bioisosteric replacement

Scaffold-hopping

SAR analysis

Structure–activity landscape

Antiviral

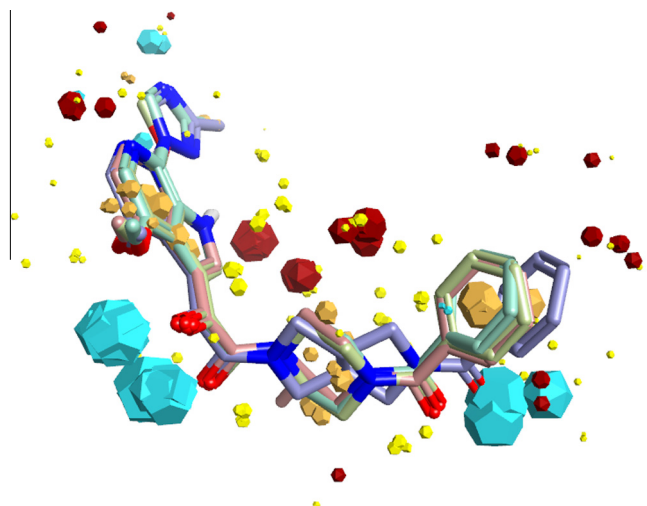
### ABSTRACT

Demand remains for new inhibitors of HIV-1 replication and the inhibition of HIV-1 entry is an extremely attractive therapeutic approach. Using field-based bioisosteric replacements, we have further extended the chemotypes available for development in the HIV-1 entry inhibitor class. Moreover, using field-based disparity analysis of the compounds, 3D structure–activity relationships were derived that will be useful in the further development of these inhibitors towards clinical utility.

© 2015 Elsevier Ltd. All rights reserved.

Inhibiting the process of entry of HIV-1 into susceptible cells remains an elusive but extremely attractive intervention point for the development of novel anti-HIV therapies. HIV-1 entry into cells is solely orchestrated by the Env complex on the surface of the virion. The Env complex is organized on the virion surface as trimeric spikes, composed of three gp120 molecules non-covalently linked to three gp41 molecules. Recently, two structures of a soluble, cleaved HIV-1 Env trimer from a clade A founder virus has been solved providing additional and much needed information on the quaternary organization of the Env complex.<sup>1–3</sup>

HIV-1 infection usually occurs only after two sequential and specific binding steps. The first interaction is between gp120 and CD4 antigen present on CD4<sup>+</sup> T cells, monocyte/macrophages, and other immune and nonimmune cells. This interaction results in a series of conformational rearrangements in gp120 that permits the second binding event to occur. This second interaction occurs between gp120 and a member of the chemokine receptor subfamily, within the large G protein–coupled family of receptors, mainly CCR5 and/or CXCR4. This interaction also promotes considerable rearrangement in gp120 and transduction of this conformational signal to gp41. This then elicits the exposure of the fusion peptide

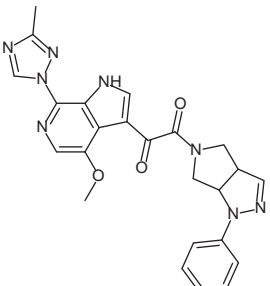
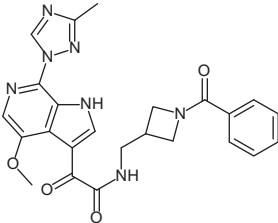
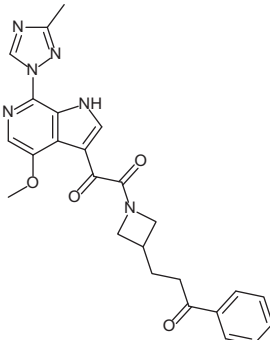
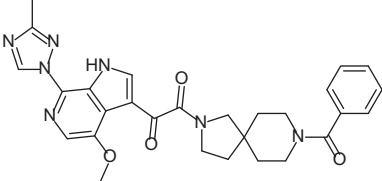
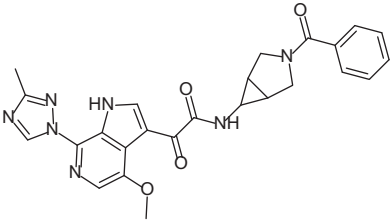
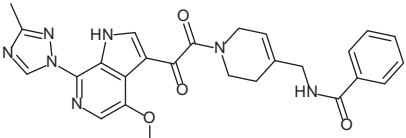


**Figure 1.** Overlaid field point representation of compounds BMS-377806, BMS488043, BMS-626529, and SC11 from the derived binding mode (Forge, UK). Red field points highlight energy minima for a positively charged probe, blue for a negative probe. Yellow spheres represent attractive van der Waals minima for a neutral probe and gold spheres represent hydrophobic centroids. Oxygen atoms are shown in red, nitrogen in blue. The size of the points is related to the strength of a potential interaction (i.e., absolute value of the field strength at that point in space).

\* Corresponding author. Tel.: +1 215 762 7234 (O), +1 215 762 4979 (lab); fax: +1 215 762 4452.

E-mail address: [scocklin@drexelmed.edu](mailto:scocklin@drexelmed.edu) (S. Cocklin).

**Table 1**Specificity and potency of compounds against HIV-1<sub>JR-CSF</sub>, HIV-1<sub>B41</sub>, HIV-1<sub>HxBc2</sub> Env, and AMLV pseudotyped HIV-1. N.A. = not active; N.D. = not determined

Compound	IC <sub>50</sub> JR-CSF (μM)	IC <sub>50</sub> B41 (μM)	IC <sub>50</sub> HxBc2 (μM)	IC <sub>50</sub> AMLV (μM)
<b>SC12</b>				
	0.008 ± 0.002	0.006 ± 0.003	0.08 ± 0.02	N.A.
<b>SC14</b>				
	2.5 ± 0.4	3.8 ± 0.4	3.8 ± 1.6	N.A.
<b>SC15</b>				
	0.003 ± 0.001	0.007 ± 0.001	0.009 ± 0.0011	N.A.
<b>SC27</b>				
	13.0 ± 9.0	3.9 ± 0.7	36 ± 21	N.A.
<b>SC28</b>				
	0.096 ± 0.019	0.085 ± 0.03	0.069 ± 0.014	N.A.
<b>SC45</b>				
	0.224 ± 0.017	0.35 ± 0.03	0.38 ± 0.03	N.A.

within the N-terminus of gp41, which through additional conformational rearrangements in gp41 facilitates fusion between the viral and cellular membranes and release of the viral core into the cell.

Several groups are actively involved in the development of small molecules targeted to gp120 that disrupt the Env molecular machine to stop HIV-1 entry into cells.<sup>4–13</sup> Despite this only one chemotype, developed by Bristol Myers Squibb, has successfully made it to clinical trials. The newest compound in the drug class, BMS-663068, a phosphonooxymethyl prodrug of BMS-626529,<sup>14</sup> recently performed favourably in a Phase IIb clinical study, highlighting the potential utility of these Env-directed entry inhibitor class of compounds (presented at the 22nd Conference on Retroviruses and Opportunistic Infections [CROI]).

Our group recently described the computational design of new compounds designed to act through a common binding site to that of the Bristol Myers Squibb piperazine-based entry inhibitors, of which BMS-663068/BMS626529 are members. Our most potent compounds, **SC11** and **SC26**, both contain a dipyrroloidine core scaffold, and specifically inhibit HIV-1<sub>JR-CSF</sub> at 0.8 and 2 nM, respectively.<sup>15</sup>

Having successfully demonstrated that scaffold-hopping of the piperazine moiety can be achieved, in this study we sought to extend the core chemotypes available for the entry inhibitor class in the hopes of improving drug-like properties. To accomplish this we performed computationally directed scaffold-hopping studies, coupled to synthesis, antiviral potency analysis and computational 3D Quantitative Structure–Activity Relationship (QSAR).

Due to the lack of structural information on the bioactive conformation of our inhibitors and the BMS piperazine based

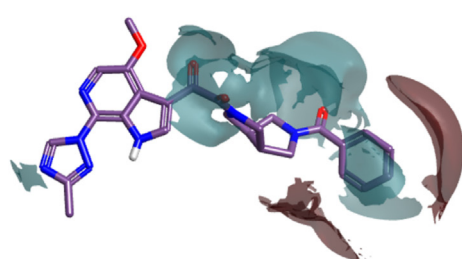
inhibitors, we first used FieldTemplater (Forge, Cresset)<sup>16–26</sup> to determine the most likely 3D conformation adopted by BMS-377806,<sup>12</sup> BMS-488043,<sup>27</sup> BMS-626529,<sup>28</sup> and **SC11/SC26**<sup>15</sup> upon binding to the HIV-1 Env target (Fig. 1). This FieldTemplater-derived 3D conformation was then used as input into Spark (Cresset, UK). Spark searches a database of up to 600,000 fragments to find bioisosteres that exhibit similar shape and electronic properties as the region of interest when placed in the context of the final molecule. To maximize the likelihood of identifying interesting potential replacements, we performed bioisosteric searches of the piperazine groups of BMS-377806, BMS-488043, and BMS-626529, in addition to the dipyrroloidine group of compounds **SC11/SC26**. The results of each search were analyzed and common structures were identified. From this analysis, four different core chemotypes were chosen for investigation based upon diversity and BIF% scores (a factor that indicates how good the replacement is in the context of the conformation of the entire molecule). Compounds containing core pyrrolo-pyrazole, azetidine, tetrahydropyridine, azabicyclo-hexane and diazaspiro-decane groups were then synthesized. First, a common head group to be used in all of the molecules was synthesized, compound **6**, according to Supplemental Scheme 1. This was subsequently used in the synthesis of compounds **SC12**, **SC14**, **SC15**, **SC27**, **SC28**, and **SC45** as outlined in Supplemental Schemes 1–7.

After successful synthesis of each of the five novel-scaffold derivatives, we then tested them for specificity and potency against HIV-1. To do this we used the HIV-1 single round infection assay. In this system, recombinant single-round infectious envelope-pseudotyped luciferase-reporter HIV-1 viruses are

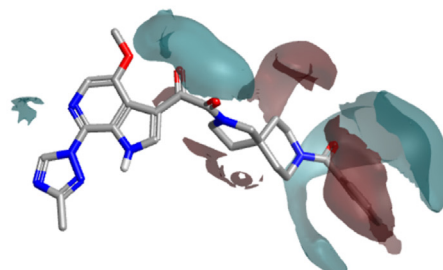
Order By	SC11	SC15	SC26	SC12	SC28	SC08	SC45	SC03	SC07	SC14	SC27	SC04
SC11		-3.6	-2.1	-5.8	-9.7	-10.4	-10.7	-6.1	-12.8	-15.3	-27.0	-12.5
SC15	3.6		0.0	-3.7	-7.1	-7.1	-9.8	-5.4	-11.0	-16.7	-22.7	-11.2
SC26	2.1	0.0		-2.4	-5.6	-8.3	-8.3	-6.0	-9.3	-12.7	-21.8	-11.6
SC12	5.8	3.7	2.4		-4.1	-3.6	-5.2	-4.1	-7.0	-10.9	-13.5	-10.4
SC28	9.7	7.1	5.6	4.1		-0.1	-1.1	-1.5	-4.0	-5.3	-8.6	-7.5
SC08	10.4	7.1	8.3	3.6	0.1		-0.9	-1.8	-5.3	-5.1	-11.4	-8.7
SC45	10.7	9.8	8.3	5.2	1.1	0.9		-1.0	-3.1	-6.2	-9.1	-6.0
SC03	6.1	5.4	6.0	4.1	1.5	1.8	1.0		-1.0	-1.9	-3.3	-7.3
SC07	12.8	11.0	9.3	7.0	4.0	5.3	3.1	1.0		-1.6	-3.8	-5.8
SC14	15.3	16.7	12.7	10.9	5.3	5.1	6.2	1.9	1.6		-2.8	-4.1
SC27	27.0	22.7	21.8	13.5	8.6	11.4	9.1	3.3	3.8	2.8		-2.1
SC04	12.5	11.2	11.6	10.4	7.5	8.7	6.0	7.3	5.8	4.1	2.1	

**Figure 2.** Disparity Matrix showing the pairwise comparisons for the compounds reported using IC<sub>50</sub> HIV-1JR-CSF as activity. Red and green boxes correspond to decreases and increases in activity between the pair, respectively. The darker the shading, the sharper the activity cliff (higher calculated Disparity). The matrix is symmetrical—for every red box, there is a corresponding green box for the comparison going in the opposite direction.

## Panel A

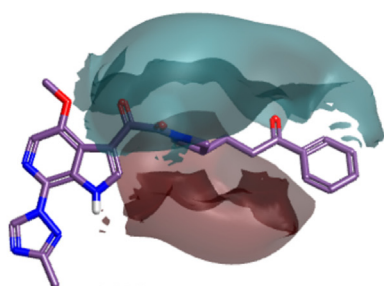


SC11  
IC<sub>50</sub> = 1 nM

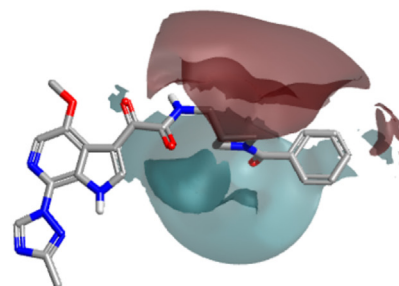


SC27  
IC<sub>50</sub> = 13 μM

## Panel B



SC15  
IC<sub>50</sub> = 2 nM



SC14  
IC<sub>50</sub> = 2.5 μM

**Figure 3.** Comparison of field differences for a selection of molecules in which the negative electrostatics over the central moiety appears to be important for activity. The field difference map displays the surfaces as relative values between pairs of molecules. The regions where the surface is displayed have stronger electrostatic fields than the corresponding regions in the compared molecule. In Panel A, **SC27** is compared to **SC11**; in the Panel B, **SC15** is compared to **SC14**. Again, IC<sub>50</sub> refers to IC<sub>50</sub> HIV-1<sub>JR-CSF</sub>.

produced by co-transfection of 293T cells with the envelope-deficient HIV-1 NL4-3 vector (pNL4-3-LucR<sup>+</sup>E<sup>-</sup>; a gift of N. R. Landau, New York University),<sup>29</sup> which carries the luciferase-reporter gene; and the HIV-1 JR-CSF, HIV-1 B41,<sup>30</sup> HIV-1 HxBc2 or amphotropic murine leukemia virus (AMLV) envelope expressing vector. These recombinant viruses are then used to infect U87.CD4.CCR5 (JR-CSF and B41 Envs) target cells or U87.CD4.CXCR4 (HxBc2 Env) and infectivity is quantified by measuring luciferase activity in cell lysates (Luciferase Assay System, Promega) using a microplate luminometer (GloMax, Promega). The effect of the compounds on the infection of target cells by AMLV Env pseudotyped recombinant HIV-1 was used to determine the specificity of the compounds to HIV-1 Env-mediated cell entry. The results of this analysis are shown in Table 1.

As can be seen from the results in Table 1, all compounds had specific anti-HIV activity but their half maximum inhibitory concentrations (IC<sub>50</sub>) showed noticeable variation. To better understand the factors driving activity of these HIV-1 entry inhibitors, including those compounds previously reported by our group, we assessed them computationally using Activity Miner and Activity Atlas (Cresset, UK). Activity Miner provides an interface for the rapid assessment of structure–activity landscapes for a set of aligned compounds in the context of activity cliffs. It achieves this by comparing pairs of molecules to find where small changes in the molecule's structure or local properties results in a large change in activity. In the software, this notion of disparity is expressed as:

$$\text{Disparity} \propto \frac{\Delta \text{Activity}}{1 - \text{Similarity}}$$

The higher the calculated disparity corresponds to a sharper change in activity between a pair of very similar molecules and hence an activity cliff.

Activity Atlas (Cresset, UK) provides a probabilistic approach to analyzing Structure Activity Relationships (SAR). Like all 3D SAR approaches, comprehensive conformation hunting and correct alignments are critical, thus, alignments were hand checked to reduce noise arising from inadequate alignments. This is a key and necessary step, since, being a probabilistic method, Activity Atlas assumes that the alignments are correct. Activity Atlas helps provide insight into what feature(s) the active compounds in a collection have in common—in essence, it summarizes the Activity Miner analysis to illuminate what activity cliffs reveal about the nature of the SAR.

Compounds **SC03**, **SC04**, **SC07**, **SC08**, **SC11** and **SC26** from our previous report,<sup>15</sup> and compounds **SC12**, **SC14**, **SC15**, **SC27**, **SC28** and **SC45** from this analysis were input into Activity Miner. From the pairwise comparisons (50% field–50% shape) a Disparity Matrix was generated (Fig. 2) which provides an overview of the dataset. For each pair, the comparison was color-coded by color and shade, with red and green meaning a decrease or increase in activity, respectively. The shading corresponds to the disparity: darker shading indicates a higher disparity, and thus, a steeper activity cliff.

As can be clearly seen in Figure 2, the highest ranked activity cliff is between molecules **SC11** (pIC<sub>50</sub> = 9.1) and **SC27** (pIC<sub>50</sub> = 4.890). This pair has a 3D Similarity of 0.844 (quite high), combined with a ΔpIC<sub>50</sub> = 4.21. When the field differences are examined, as shown in Figure 3, it can be observed that the

electron density spanning the dipyrrolidine in **SC11** is absent in the central diazaspino-decane group of **SC27**. This suggests that electron density in the center of the molecule may be important for activity.

This observation is conserved in the comparisons of **SC15** and **SC26** to **SC27**, with the higher potency compounds having this region of electron density. Furthermore, this observation is even borne out in the comparison of **SC15** to **SC14**. **SC14** and **SC15** share a core azetidine moiety but differ in its orientation. Again, the reduction of negativity in the core region is seen in the lower potency compound **SC14** but maintained in the highly active **SC15** compound.

Comparison of **SC11** to its parental compound **SC04** ( $IC_{50}$  HIV-1<sub>JR-CSF</sub> = 100  $\mu$ M), highlights key field differences that could explain the corresponding 5-order of magnitude difference in activity (Fig. 4). Most striking are the differences between the 'head regions' of the compounds. The acenaphthene head group of **SC04** shows an intact  $\pi$ -cloud, as well as positivity associated with the in-plane hydrogens that is not observed in the azaindole group of the more active **SC11** (Fig. 4, Panel B).

Evaluating the complex structure–activity relationship for this set of compounds, which have only loosely related 2D structure based on Tanimoto similarity scores (based on Merck Atom Pairs), resulted in a number of comparisons to examine in Activity Miner. The visualization of single-pair comparisons provides plenty of insight for molecule pairs with only minor structural or featural changes resulting in activity cliffs. However, when examining more complex datasets containing multiple chemotypes with multiple

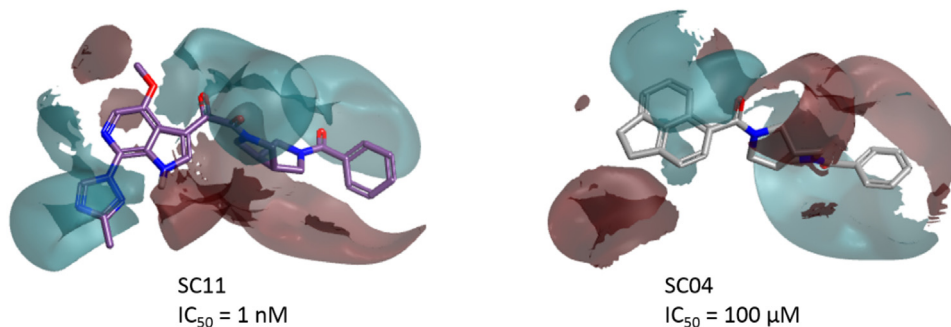
simultaneous scaffold modifications, it is more convenient and illuminative to summarize the pair-wise information using Activity Atlas (Cresset, UK).

Activity Atlas analyzes SAR by employing a Bayesian approach to qualitatively attain a global overview of available 3D structure and activity information. Effectively, this approach automates and summarizes the pair comparisons that could be examined and exploited for SAR understanding in Activity Miner. The aim of Activity Atlas is to: determine what electrostatic/hydrophobic/shape features active molecules in the data set have in common; to understand what the activity cliffs suggest about the SAR; and finally, to be able to assess how well the compounds cover available chemical (or feature) space.

Once the Activity Atlas calculated average field contributions to activity for the data set are plotted, one can look at new molecules in the context of these averages to assess suitability for progression.

Examining three of the compounds in the dataset with high, mid, and low potencies in the context of the average field contributions (Fig. 5, Panel A), we see that one of the most active compounds (**SC26**), shows a field pattern that aligns well with the average electrostatics. **SC14**, which has mid-range activity ( $IC_{50}$  JR-CSF = 2.5  $\mu$ M), has a field point pattern which aligns acceptably in some areas, but doesn't meet the negative electrostatic directionality associated with the carbonyl group shown on the right. Finally, **SC04**, with  $IC_{50}$  of 100  $\mu$ M, shows reasonable field matching across the core, but the acenaphthene 'head region' lacks much of the fields present in the higher potency molecules (Fig. 5, Panel B).

Panel A



Panel B

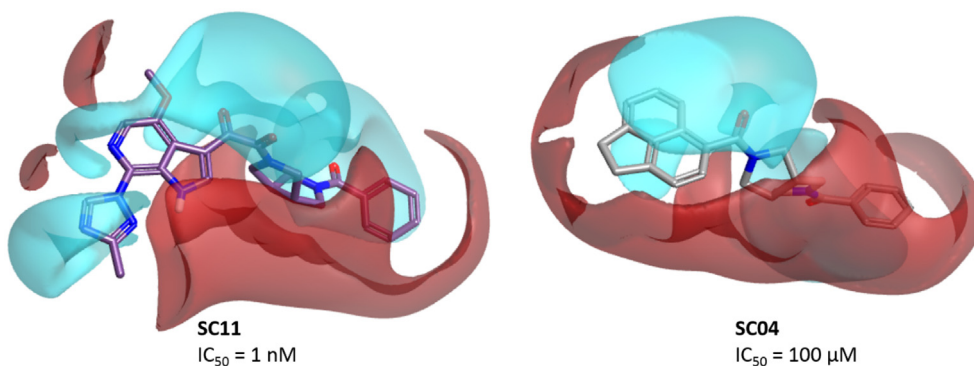
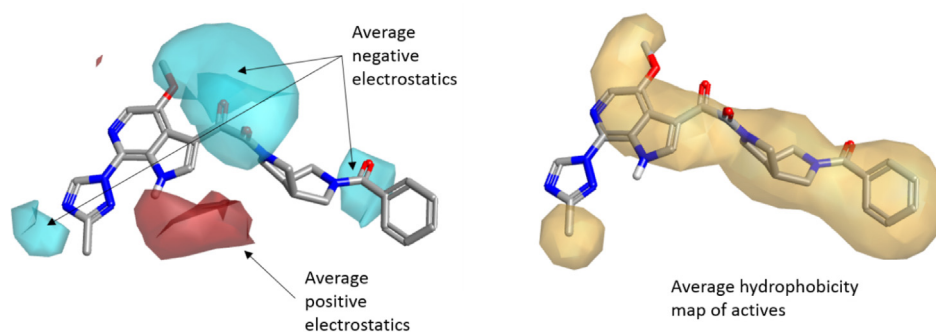


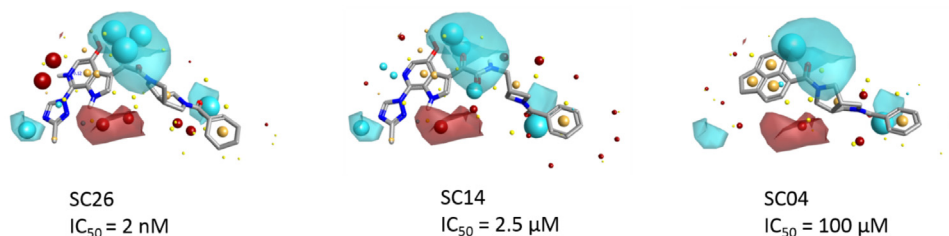
**Figure 4.** (Panel A) Comparing the field differences between **SC11** and **SC04**. The  $\pi$ -cloud associated with the fused rings remains intact, whereas in the more active **SC11**, that electron density has been pulled out of the region. (Panel B) Comparison of the calculated electrostatic surfaces for **SC11** and **SC04**. Notice the intact  $\pi$ -cloud of the acenaphthene, as well as the positive field associated with the in-plane hydrogens, which leaves them available for potential hydrogen bonding.



## Panel A



## Panel B



## Panel C

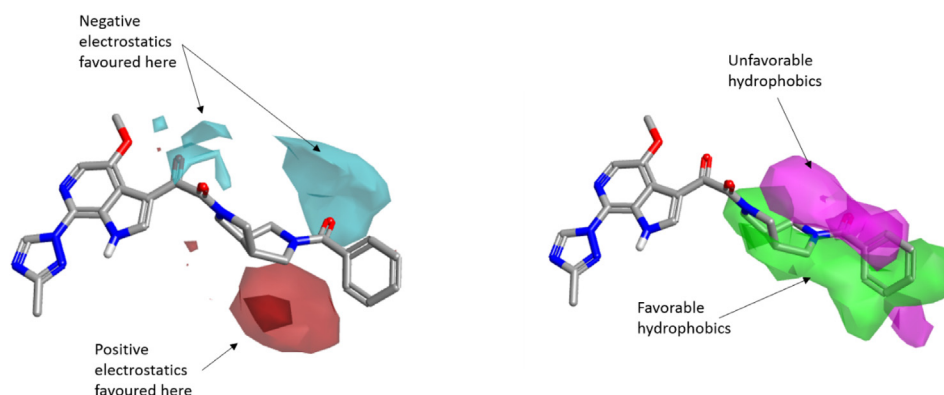


**Figure 5.** (Panel A) Compound **SC11** showing the average electrostatics and average hydrophobic regions based on the Activity Atlas summary of active molecules in the dataset. (Panel B) Assessing three compounds in the context of the average electrostatics associated with activity based on the dataset. The higher active molecules have better correlation with the average fields for actives (shown in Panel A), while the less active compounds miss critical features of the SAR. Red and blue maps depict the average positive and negative electrostatics associated with active molecules, based on the dataset.  $IC_{50}$  refers to  $IC_{50}$  HIV-1<sub>JR-CSF</sub>. (Panel C) Summary graphic of the activity cliffs found by pairwise comparisons in Activity Miner and summarized in Activity Atlas. The maps in this graphic show the key features that drive activity, as determined from the alignment of the reported compounds. Note that ‘more negative’ can also mean ‘less positive’, and vice versa.

When the activity cliff information is summarized using Activity Atlas (Fig. 5, Panel C), it is seen that there are regions with specific electrostatic conditions, as well as hydrophobicity considerations. In essence, these regions qualitatively express our 3D SAR in a graphical fashion and provide a blueprint for the design of further analogues.

In summary, we have extended our previous work using computational means to diversify the core scaffolds in the entry inhibitor class, identifying 5 new core chemotypes. Computational analysis of these core chemotype diversified inhibitors has provided a blueprint that can be used in the design of next generation entry inhibitors to improve the potency. Taken together, the results from this study validate the combined use of field-based bioisosteric replacement and field-based disparity analysis as a means to further the potential utility of Env-targeted HIV-1 entry

inhibitors. Future studies in our group will include assessment of the drug-like properties of these new chemotypes, modulation and optimization of their potencies based upon SAR relationships derived in this study and simultaneously against genetically distinct isolates, and detailed mechanism of action studies, including structural studies.

### Acknowledgment

This work was supported by NIH/NIAID Grant 1R21AI104354-01A1 (Cocklin, PI) and W. W. Smith Charitable Trust Grant #A1301 (Cocklin, PI). We'd like to thank Pavel Pugachev and John P. Moore (Department of Microbiology and Immunology, Weill Medical College of Cornell University, New York, NY 10021, USA) for the generous gift of the B41 gp160 expression plasmid.

## Supplementary data

Supplementary data associated with this article can be found, in the online version, at <http://dx.doi.org/10.1016/j.bmcl.2015.10.080>.

## References and notes

1. Lyumkis, D.; Julien, J. P.; de Val, N.; Cupo, A.; Potter, C. S.; Klasse, P. J.; Burton, D. R.; Sanders, R. W.; Moore, J. P.; Carragher, B.; Wilson, I. A.; Ward, A. B. *Science* **2013**, *342*, 1484.
2. Julien, J. P.; Cupo, A.; Sok, D.; Stanfield, R. L.; Lyumkis, D.; Deller, M. C.; Klasse, P. J.; Burton, D. R.; Sanders, R. W.; Moore, J. P.; Ward, A. B.; Wilson, I. A. *Science* **2013**, *342*, 1477.
3. Pancera, M.; Zhou, T.; Druz, A.; Georgiev, I. S.; Soto, C.; Gorman, J.; Huang, J.; Acharya, P.; Chuang, G. Y.; Ofek, G.; Stewart-Jones, G. B.; Stuckey, J.; Bailer, R. T.; Joyce, M. G.; Louder, M. K.; Tumba, N.; Yang, Y.; Zhang, B.; Cohen, M. S.; Haynes, B. F.; Mascola, J. R.; Morris, L.; Munro, J. B.; Blanchard, S. C.; Mothes, W.; Connors, M.; Kwong, P. D. *Nature* **2014**.
4. Courter, J. R.; Madani, N.; Sodroski, J.; Schon, A.; Freire, E.; Kwong, P. D.; Hendrickson, W. A.; Chaiken, I. M.; Lalonde, J. M.; Smith, A. B., 3rd. *Acc. Chem. Res.* **2014**.
5. Kwon, Y. D.; LaLonde, J. M.; Yang, Y.; Elban, M. A.; Sugawara, A.; Courter, J. R.; Jones, D. M.; Smith, A. B., 3rd; Debnath, A. K.; Kwong, P. D. *PLoS One* **2014**, *9*, e85940.
6. Li, Z.; Zhou, N.; Sun, Y.; Ray, N.; Lataillade, M.; Hanna, G. J.; Krystal, M. *Antimicrob. Agents Chemother.* **2013**, *57*, 4172.
7. Lalonde, J. M.; Le-Khac, M.; Jones, D. M.; Courter, J. R.; Park, J.; Schon, A.; Princiotto, A. M.; Wu, X.; Mascola, J. R.; Freire, E.; Sodroski, J.; Madani, N.; Hendrickson, W. A.; Smith, A. B., 3rd. *ACS Med. Chem. Lett.* **2013**, *4*, 338.
8. Curreli, F.; Choudhury, S.; Pyatkin, I.; Zagorodnikov, V. P.; Bulay, A. K.; Altieri, A.; Kwon, Y. D.; Kwong, P. D.; Debnath, A. K. *J. Med. Chem.* **2012**, *55*, 4764.
9. Williams, D. H.; Adam, F.; Fenwick, D. R.; Fok-Seang, J.; Gardner, I.; Hay, D.; Jaessh, R.; Middleton, D. S.; Mowbray, C. E.; Parkinson, T.; Perros, M.; Pickford, C.; Platts, M.; Randall, A.; Siddle, D.; Stephenson, P. T.; Tran, T. D.; Vuong, H. *Bioorg. Med. Chem. Lett.* **2009**, *19*, 5246.
10. Zhao, Q.; Ma, L.; Jiang, S.; Lu, H.; Liu, S.; He, Y.; Strick, N.; Neamati, N.; Debnath, A. K. *Virology* **2005**, *339*, 213.
11. Si, Z.; Madani, N.; Cox, J. M.; Chruma, J. J.; Klein, J. C.; Schon, A.; Phan, N.; Wang, L.; Biorn, A. C.; Cocklin, S.; Chaiken, I.; Freire, E.; Smith, A. B., 3rd; Sodroski, J. G. *Proc. Natl. Acad. Sci. U.S.A.* **2004**, *101*, 5036.
12. Lin, P. F.; Blair, W.; Wang, T.; Spicer, T.; Guo, Q.; Zhou, N.; Gong, Y. F.; Wang, H. G.; Rose, R.; Yamanaka, G.; Robinson, B.; Li, C. B.; Fridell, R.; Deminie, C.; Demers, G.; Yang, Z.; Zadjura, L.; Meanwell, N.; Colonna, R. *Proc. Natl. Acad. Sci. U.S.A.* **2003**, *100*, 11013.
13. Herschhorn, A.; Gu, C.; Espy, N.; Richard, J.; Finzi, A.; Sodroski, J. G. *Nat. Chem. Biol.* **2014**, *10*, 845.
14. Nettles, R. E.; Schurmann, D.; Zhu, L.; Stonier, M.; Huang, S. P.; Chang, I.; Chien, C.; Krystal, M.; Wind-Rotolo, M.; Ray, N.; Hanna, G. J.; Bertz, R.; Grasela, D. J. *Infect. Dis.* **2012**, *206*, 1002.
15. Tuyishime, M.; Danish, M.; Princiotto, A.; Mankowski, M. K.; Lawrence, R.; Lombart, H. G.; Esikov, K.; Berniac, J.; Liang, K.; Ji, J.; Ptak, R. G.; Madani, N.; Cocklin, S. *Bioorg. Med. Chem. Lett.* **2014**, *24*, 5439.
16. Cheeseright, T.; Mackey, M.; Rose, S.; Vinter, A. *J. Chem. Inf. Model.* **2006**, *46*, 665.
17. Cheeseright, T.; Mackey, M.; Rose, S.; Vinter, A. *Expert Opin. Drug Discov.* **2007**, *2*, 131.
18. Cheeseright, T. J.; Holm, M.; Lehmann, F.; Luik, S.; Gottert, M.; Melville, J. L.; Laufer, S. *J. Med. Chem.* **2009**, *52*, 4200.
19. Cheeseright, T. J.; Mackey, M. D.; Melville, J. L.; Vinter, J. G. *J. Chem. Inf. Model.* **2008**, *48*, 2108.
20. Cheeseright, T. J.; Mackey, M. D.; Scoffin, R. A. *Curr. Comput. Aided Drug Des.* **2011**, *7*, 190.
21. Collins, J. C.; Armstrong, A.; Chapman, K. L.; Cordingley, H. C.; Jaxa-Chamiec, A. A.; Judd, K. E.; Mann, D. J.; Scott, K. A.; Tralau-Stewart, C. J.; Low, C. M. R. *MedChemComm* **2013**, *4*, 1148.
22. Kirpotina, L. N.; Khlebnikov, A. I.; Schepetkin, I. A.; Ye, R. D.; Rabiet, M. J.; Jutila, M. A.; Quinn, M. T. *Mol. Pharmacol.* **2010**, *77*, 159.
23. Low, C. M.; Buck, I. M.; Cooke, T.; Cushnir, J. R.; Kalindjian, S. B.; Kotecha, A.; Pether, M. J.; Shankley, N. P.; Vinter, J. G.; Wright, L. *J. Med. Chem.* **2005**, *48*, 6790.
24. Low, C. M.; Vinter, J. G. *J. Med. Chem.* **2008**, *51*, 565.
25. Mackey, M. D.; Melville, J. L. *J. Chem. Inf. Model.* **2009**, *49*, 1154.
26. Webster, S. P.; Binnie, M.; McConnell, K. M.; Sooy, K.; Ward, P.; Greaney, M. F.; Vinter, A.; Pallin, T. D.; Dyke, H. J.; Gill, M. I.; Warner, I.; Seckl, J. R.; Walker, B. R. *Bioorg. Med. Chem. Lett.* **2010**, *20*, 3265.
27. Yang, Z.; Zadjura, L. M.; Marino, A. M.; D'Arienzo, C. J.; Malinowski, J.; Gesenberg, C.; Lin, P. F.; Colonna, R. J.; Wang, T.; Kadow, J. F.; Meanwell, N. A.; Hansel, S. B. *J. Pharm. Sci.* **2010**, *99*, 2135.
28. Nowicka-Sans, B.; Gong, Y. F.; McAuliffe, B.; Dicker, I.; Ho, H. T.; Zhou, N.; Eggers, B.; Lin, P. F.; Ray, N.; Wind-Rotolo, M.; Zhu, L.; Majumdar, A.; Stock, D.; Lataillade, M.; Hanna, G. J.; Matiskella, J. D.; Ueda, Y.; Wang, T.; Kadow, J. F.; Meanwell, N. A.; Krystal, M. *Antimicrob. Agents Chemother.* **2012**, *56*, 3498.
29. Connor, R. I.; Chen, B. K.; Choe, S.; Landau, N. R. *Virology* **1995**, *206*, 935.
30. Pugach, P.; Ozorowski, G.; Cupo, A.; Ringe, R.; Yasmeen, A.; de Val, N.; Derking, R.; Kim, H. J.; Korzun, J.; Golabek, M.; de Los Reyes, K.; Ketts, T. J.; Julien, J. P.; Burton, D. R.; Wilson, I. A.; Sanders, R. W.; Klasse, P. J.; Ward, A. B.; Moore, J. P. *J. Virol.* **2015**, *89*, 3380.